



# Investigation of the Behavior of Steel Plate Shear Walls Considering Double Corrugated Low-Yield-Point Steel Infill Plate

Leila Hosseinzadeh<sup>1</sup> · Denise-Penelope N. Kontoni<sup>2,3</sup> · Behnam Babaei<sup>1</sup>

Received: 21 January 2023 / Revised: 7 May 2023 / Accepted: 31 May 2023 / Published online: 20 June 2023  
© The Author(s) 2023

## Abstract

During the last three decades, interest in the application of steel shear walls has increased worldwide. Steel shear walls are used as stiffened and unstiffened walls. One of the main shortcomings of the steel plate shear wall (SPSW) is the infill plate buckling mainly under lateral wind and seismic loads. One of the useful solutions to prevent lateral buckling is the use of walls with corrugated plates. In this research, the behavior of a steel shear wall consisting of two corrugated plates was investigated in the two material cases of the conventional ASTM A36 steel and the low-yield-point (LYP) steel. The use of steel with low yield strength improves the seismic performance of the steel shear wall system. In this study, the effect of the corrugation angle and aspect ratio of the plate were investigated. The results showed that the effect of corrugation angle on the structural parameters of walls with LYP steel is greater than that of walls with A36 steel. By increasing the corrugation angle from 30° to 60°, the elastic stiffness of A36 and LYP walls decreased about 24 and 36%, respectively, and the response modification factor ( $R_u$ ) of A36 and LYP walls decreased by about 24 and 56%. The corrugation angle has a lower effect on the ultimate strength and energy absorption. Investigating the effect of aspect ratio showed that increasing the aspect ratio improves the seismic performance of the wall.

**Keywords** Steel plate shear wall (SPSW) · Stiffness · Ultimate strength · Energy absorption · Double corrugated plate · Low-yield-point (LYP) steel

## 1 Introduction

Steel plate shear wall (SPSW) systems have suitable performance in experimental and numerical studies. This system has enjoyed high stiffness and strength and considerable energy absorption. In the SPSW system, the infill plate plays an important role as a ductile lateral force-

resisting system [1–3]. Buckling and dynamics are pressing problems in many engineering applications, e.g., thin-frame, column-like, thin-wall, and aerospace/automotive structures. These types of structures are often susceptible to instability, failure due to buckling, and dynamics issues [4, 5]. In steel shear walls, due to the low buckling capacity of the infill plate, buckling appears under the service load, which is a problem mainly under wind loads. To overcome this problem, some ideas have been presented, such as: utilizing stiffener, covering infill plates with concrete [6] or Fiber Reinforced Polymer (FRP) [7], utilizing semi-supported SPSW [8], and utilizing corrugated infill plates [9]. Among the proposed methods, utilizing corrugated infill plates is the most practical and easier to build than other ones.

The steel plate shear wall utilizing corrugated plates (C-SPSW) has shown acceptable seismic behavior. The C-SPSW enjoys larger out-of- and in-plane stiffness and lateral resistance than the conventional steel plate shear walls (SPSWs) under lateral loading [10]. The shape of

✉ Denise-Penelope N. Kontoni  
kontoni@uop.gr; kontoni.denise@ac.eap.gr

Leila Hosseinzadeh  
l.hosseinzadeh@iaut.ac.ir

Behnam Babaei  
b.babaei1996@gmail.com

<sup>1</sup> Department of Civil Engineering, Tabriz Branch, Islamic Azad University, Tabriz, Iran

<sup>2</sup> Department of Civil Engineering, School of Engineering, University of the Peloponnese, 26334 Patras, Greece

<sup>3</sup> School of Science and Technology, Hellenic Open University, 26335 Patras, Greece

corrugated infill plates was sinusoidal [11], rectangular [12], or trapezoidal corrugations [13]. The trapezoidal corrugated form was most commonly utilized in practice [14].

The use of corrugated plates as shear-resistant members was first developed in the late 1930s by Bergman and Reissner [15]. After the finding of Bergman, the shear buckling of the corrugated plates was widely studied [16–21].

The behavior of the C-SPSW was investigated comprehensively [22, 23] and research was focused on predicting the load–displacement curve of the system under monotonic loading.

Several researchers [24–31] studied the hysteretic behavior of the C-SPSW experimentally and numerically, and they confirmed the capability of the C-SPSW as a successful system under lateral loading.

Although the C-SPSW system has significant advantages but corrugated plates are produced from flat steel plates using cold rolling machines, so their thickness must be limited. The maximum thickness of corrugated plates used in practice is 8 mm. If high ultimate strength is required in the design, a thick corrugated plate should be used. To overcome the problem, Tong et al. [32] proposed utilizing double corrugated plates in the C-SPSW system. He investigated the behavior of the double corrugated plates in C-SPSW numerically and parametrically [33, 34].

The present study intends to provide an investigation into the behavior of double corrugated steel plate shear walls (DC-SPSWs). Although double corrugated plate has high elastic stiffness and strength, it suffered from low ductility due to the buckling of the infill plate. This dilemma was confirmed by Tong et al. [33]. To overcome the problem, an infill plate made of low-yield-point (LYP) steel was proposed. Since LYP steel possesses lower strength than A36, it is expected to have higher ductility. Herein, the finite element method is used to simulate the double corrugated steel plate shear wall (DC-SPSW). The effects of the corrugated angle ( $\theta$ ), the ratio of length (L) to height (H), and the steel type (A36 and LYP) of the infill plate on the behavior of the DC-SPSW are investigated.

## 2 Method of Study

In this study, the behavior of SPSW, composed of double corrugated plates for infill plate (DC-SPSW) made of low-yield-point steel (LYP) or ordinary steel (ASTM A36), is investigated numerically and parametrically. To do this, first, a wall with  $L = H = 3000$  mm and A36 steel is designed based on Ref. [32]. The designed boundary frame is shown in Fig. 1. In this model, the thickness of the double infill plate was measured as  $2 \times 2$  mm. The

boundary frame was designed according to the stress transferred from the infill plate. To do so, it was designed based on the AISC-guide 20 [35]. The wall was determined with a corrugated angle  $\theta$  of 30 degrees, and the corrugations were considered horizontal. To investigate the effect of the LYP steel on the behavior of the wall system, by keeping the strength of the plate, its thickness was increased by  $\frac{F_{yA36}}{F_{yLYP}}$ , where the  $F_{yA36}$  and  $F_{yLYP}$  are the yielding stress of infill wall with A36 steel and LYP steel, respectively [36]. Since the ratio is  $\frac{F_{yA36}}{F_{yLYP}} = 2.5$ , for models with LYP steel, double corrugated plates with a thickness of  $2 \times 5$  mm were used. For both walls with different yielding stress, the lateral strength of the infill plate is the same.

To investigate the effect of the L/H ratio with a fixed height of 3000 mm, the walls with  $L/H = 1, 1.5,$  and  $2$  were analyzed for both LYP steel and A36 steel. Also, models with  $\theta$  equal to 30, 45, 60, and 90 (degrees) were investigated.

## 3 Numerical Study

### 3.1 Numerical Models

The introduced 24 numerical models are listed in Table 1, where for each numerical model, a name has been designed. The first letters of the name stand for the Double Corrugated (DC) SPSW. The second and third letter represents the L/H ratio and  $\theta$ , respectively. Finally, the last letter, A and L, shows the material of the infill plates that are A36 and LYP, respectively.

The finite element (FE) method and the ABAQUS software [37] were used to simulate the DC-SPSW through a set of one-story, one-bay frame models. Beams, columns, and corrugated infill panels were modeled with the four-node shell element (S4R). This element is a doubly curved thin or thick shell, with reduced integration, hourglass control, and finite membrane strain. Each element node has six degrees of freedom [38, 39]. The finite element models were loaded under horizontal load. Geometric nonlinearities were applied in the analysis of the finite element models under monotonic loading. The stress–strain curve of the material was modeled with a bilinear representation. Therefore, the material nonlinearities were applied in all the finite element analyses.

### 3.2 Verification of Results

In this study, the experimental investigation carried out by Hosseinzadeh et al. [9] was used for the verification of the finite element (FE) model, as shown in Fig. 2. The

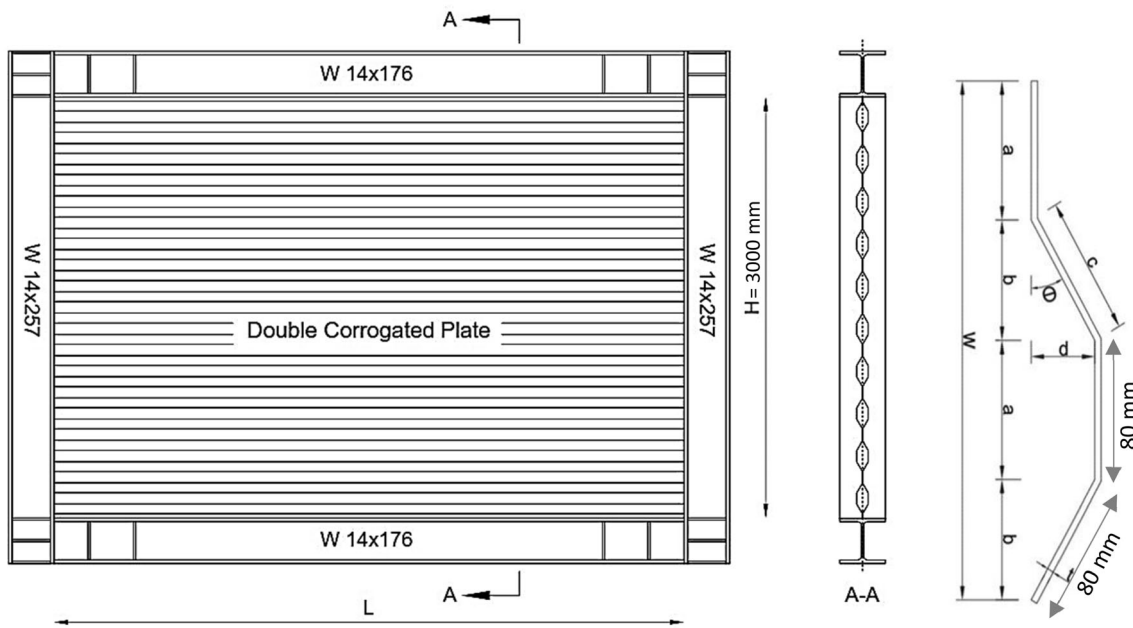


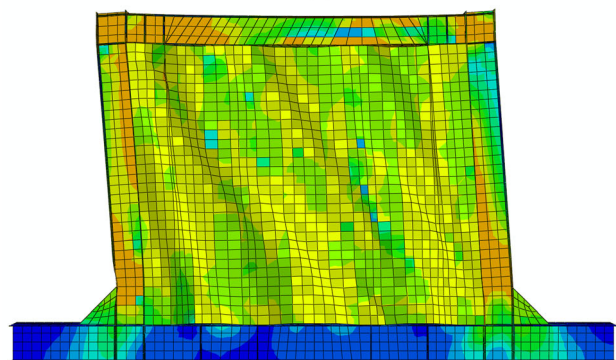
Fig. 1 Schematic view of DC-SPSW

Table 1 Numerical model properties

No	Model	L (m)	L/H	$\theta$ (Deg)	Infill plate steel
1	DC-1-30-A	3.00	1.00	30	A36
2	DC-1-45-A	3.00	1.00	45	A36
3	DC-1-60-A	3.00	1.00	60	A36
4	DC-1-90-A	3.00	1.00	90	A36
5	DC-1-30-L	3.00	1.00	30	LYP
6	DC-1-45-L	3.00	1.00	45	LYP
7	DC-1-60-L	3.00	1.00	60	LYP
8	DC-1-90-L	3.00	1.00	90	LYP
9	DC-1.5-30-A	4.50	1.50	30	A36
10	DC-1.5-45-A	4.50	1.50	45	A36
11	DC-1.5-60-A	4.50	1.50	60	A36
12	DC-1.5-90-A	4.50	1.50	90	A36
13	DC-1.5-30-L	4.50	1.50	30	LYP
14	DC-1.5-45-L	4.50	1.50	45	LYP
15	DC-1.5-60-L	4.50	1.50	60	LYP
16	DC-1.5-90-L	4.50	1.50	90	LYP
17	DC-2-30-A	6.00	2.00	30	A36
18	DC-2-45-A	6.00	2.00	45	A36
19	DC-2-60-A	6.00	2.00	60	A36
20	DC-2-90-A	6.00	2.00	90	A36
21	DC-2-30-L	6.00	2.00	30	LYP
22	DC-2-45-L	6.00	2.00	45	LYP
23	DC-2-60-L	6.00	2.00	60	LYP
24	DC-2-90-L	6.00	2.00	90	LYP



(a)



(b)

Fig. 2 a Experimental model; b FE model

specimens of C-SPSW with one-story and single-bay in half-scale were tested. The load–displacement curves and the model’s overall behavior were compared with those of the experimental studies. The results, as depicted in Fig. 3, show a very good comparison between the experimental results and the FE results.

### 3.3 Loading Regime and Boundary Conditions

Lateral loads are applied to the beam-column connections and are gradually increased from zero to a magnitude beyond the system’s capacity. The ultimate displacement limit is considered to occur at a drift ratio of 2.5% per ASCE/SEI 7–22 [40]. To simulate the fixed condition of the column-to-base plate connections, the bottom nodes of both columns’ flanges and webs are restrained from displacement and rotation in all directions. To simulate the constraints imposed by slabs of the story floors, the out-of-plane displacements of beam webs were restrained from translation in the global z-direction. The connections of the two corrugated plates are completely interlocked, and the screw connections are omitted to simplify the calculations.

### 3.4 Materials Properties

The ASTM A36 and LYP steels were selected for numerical models. The boundary frame was made of ASTM A36 steel, and the wall plate was made of ASTM A36 and LYP steel. The material stress–strain behavior curves [35] are shown in Fig. 4, where Young’s modulus is 200 GPa, and Poisson’s ratio is 0.3.

### 3.5 Defining the Seismic Behavior Parameters

To estimate the seismic parameters, the actual load–displacement response curves are usually idealized, as

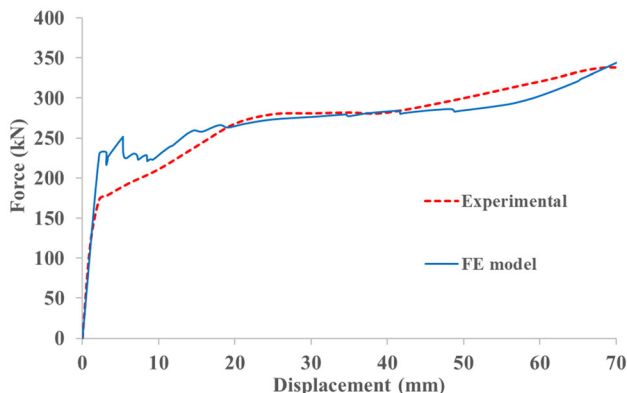


Fig. 3 Comparison of the load–displacement curves between the experimental [9] and the FE results

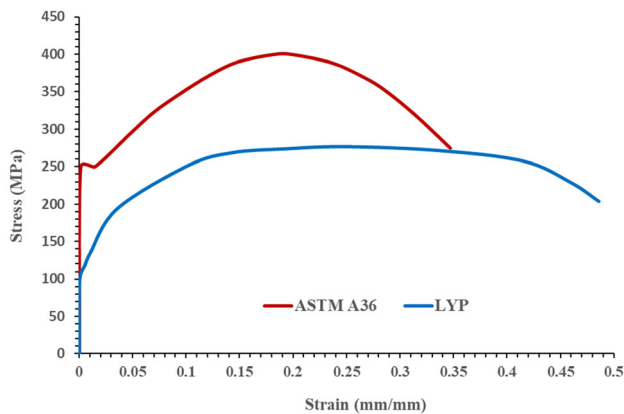


Fig. 4 The stress–strain behavior curves of the material

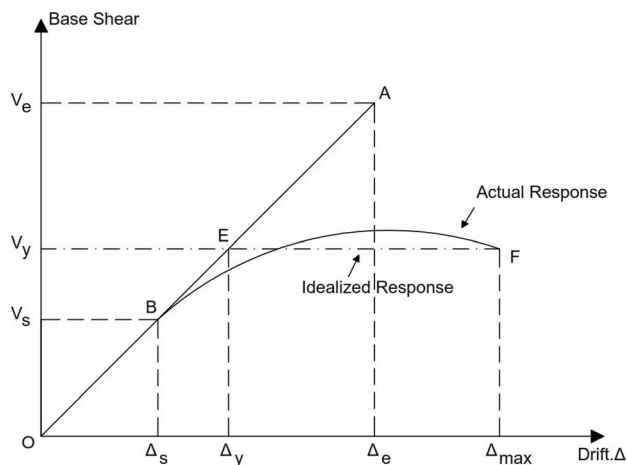


Fig. 5 Actual and idealized response curves of a common structure

illustrated in Fig. 5. This idealization is based on the following assumptions and definitions:

- The maximum displacement of the structure,  $\Delta_{max}$ , will be considered based on the requirements of the local regulations.
- The ductility factor is  $\mu = \Delta_{max}/\Delta_y$ .
- The elastic stiffness is equal to the initial slope of the load–deformation curve and is  $K = V_y/\Delta_y$ .
- The over-strength factor,  $\Omega$ , is defined as the ratio of yield resistance,  $V_y$ , to the lateral force corresponding to the first yield of structure,  $V_s$ .
- The energy absorbed by the system,  $E$ , is equal to the closed area under the load–displacement curve.
- The response modification factor is  $R_u = V_e/V_s$



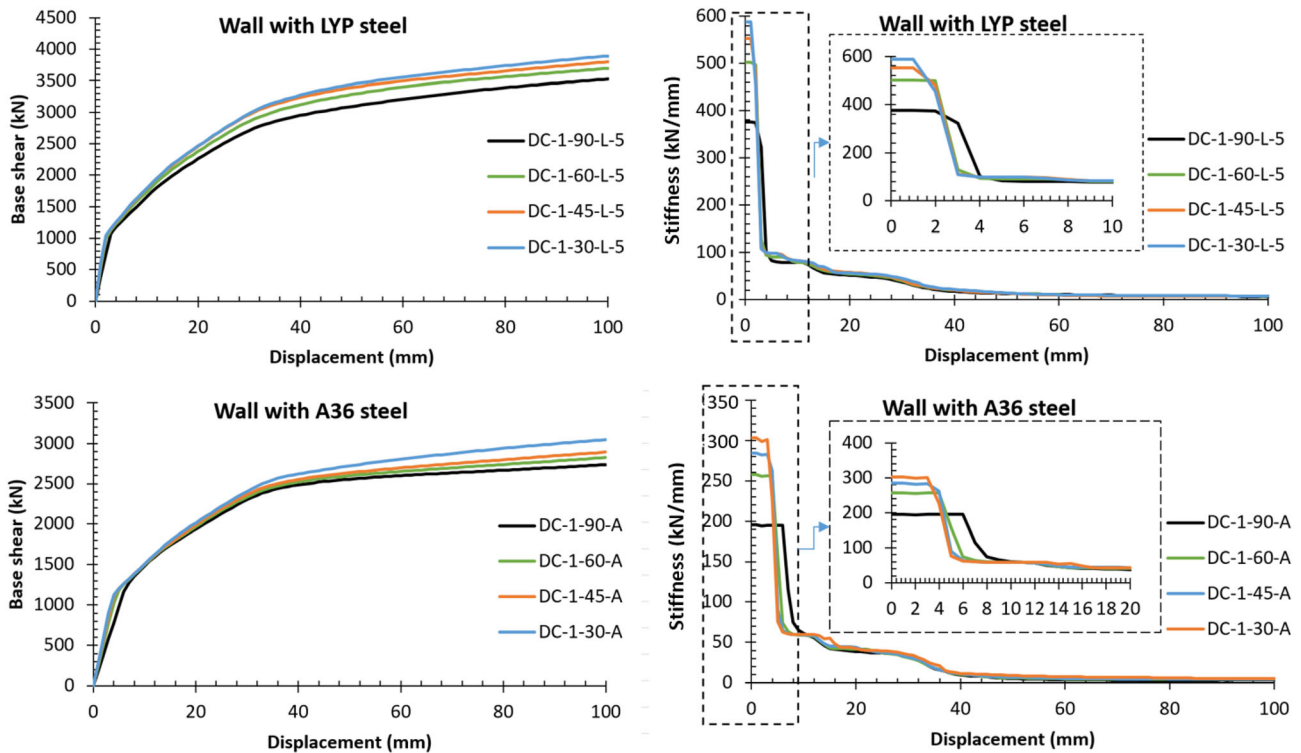


Fig. 6 Comparing the pushover curve of the FE models

Table 2 Structural parameters of numerical models with L/H = 1

Models	$\Delta_s$ (mm)	$V_s$ (kN)	$\Delta_y$ (mm)	$V_u$ (kN)	K (kN/mm)	E (kN.m)	$\Omega$	$R_u$
DC-1-30-A	3.40	992.87	9.88	2993.91	302.93	247.28	3.02	12.33
DC-1-45-A	3.85	1070.72	10.02	2844.90	283.84	238.90	2.66	10.88
DC-1-60-A	4.03	1029.86	10.80	2780.89	257.39	234.92	2.70	10.68
DC-1-90-A	6.04	1172.66	13.81	2700.49	195.49	229.32	2.30	8.07
DC-1-30-L	1.30	724.85	6.49	3819.11	588.46	311.03	5.27	26.40
DC-1-45-L	1.75	912.79	6.75	3729.96	552.84	306.21	4.09	20.16
DC-1-60-L	1.84	919.58	7.24	3632.42	501.73	297.29	3.95	18.78
DC-1-90-L	2.70	976.99	9.21	3463.71	375.95	281.64	3.55	14.89

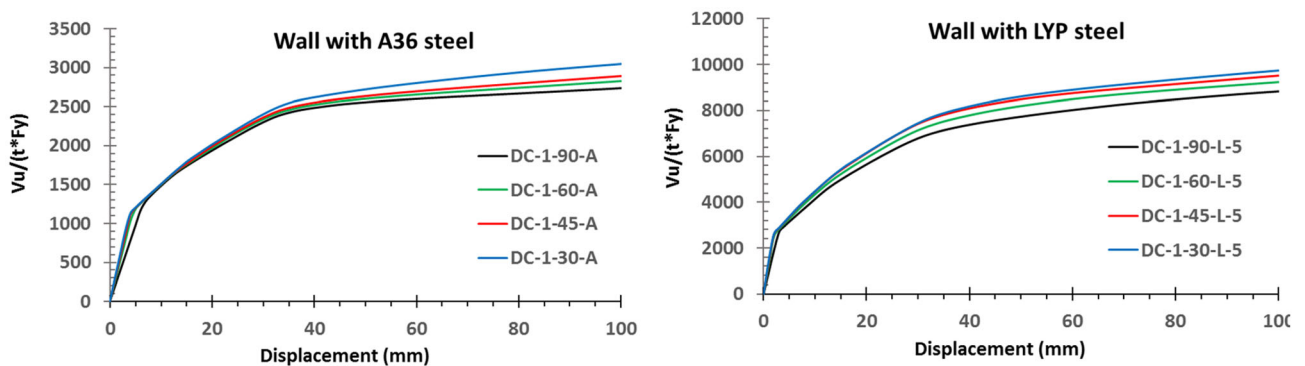


Fig. 7 Comparing the normalized response curves

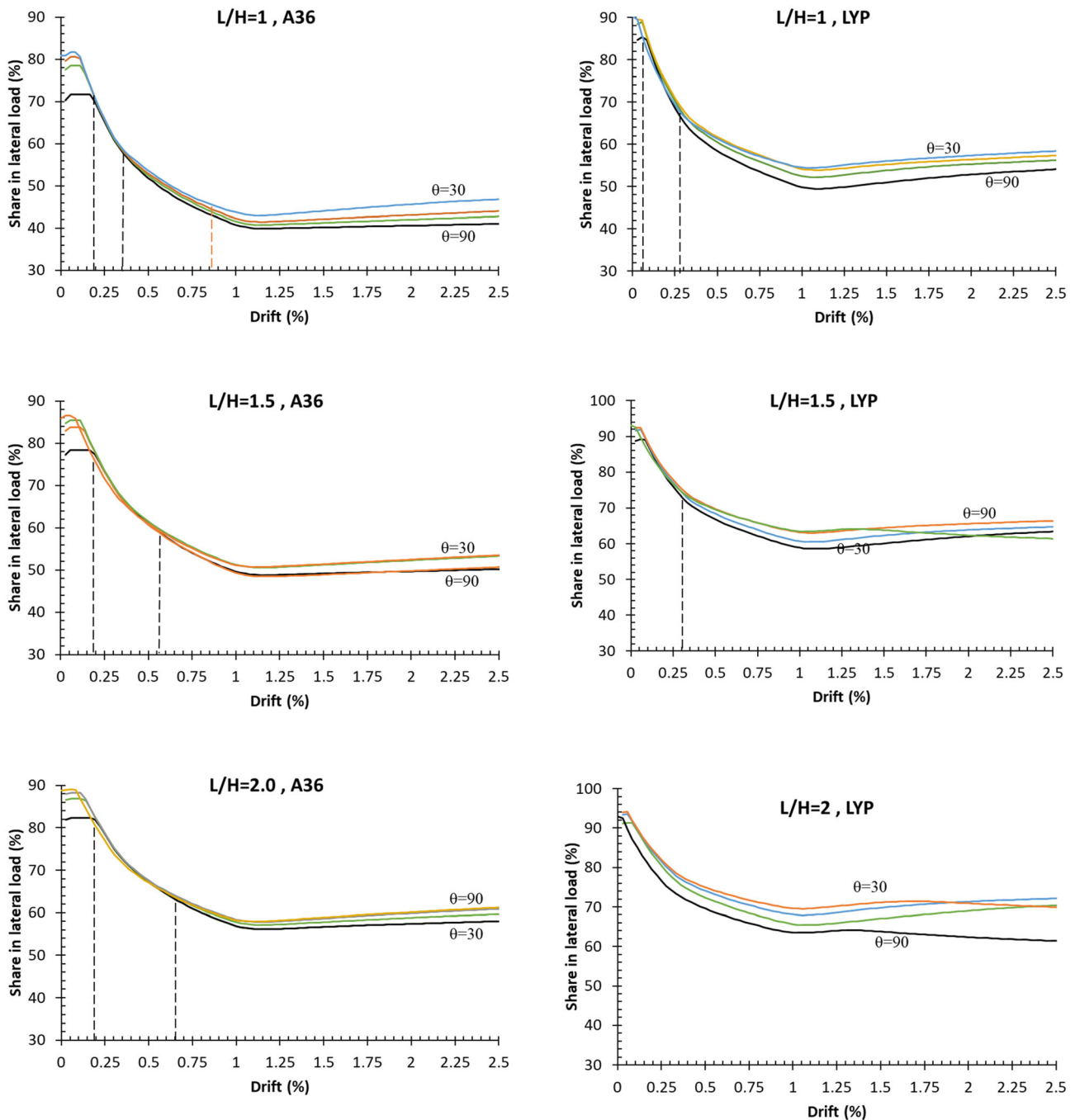


Fig. 8 The effect of angle  $\theta$  on the infill plate behavior

## 4 Discussions and Results

### 4.1 General Finding

Load versus displacement and also stiffness versus displacement plots, which are drawn in Fig. 6, reveal some valuable information conserving the behavior of structures. In addition, the structural parameters are listed in Table 2. According to Fig. 6 and Table 2, both the corrugated angle

and infill materials affect the behavior of walls. An overall view reveals that the larger ultimate strength, energy dissipating capacity, and elastic stiffness are obtained by the corrugated plate with an angle of 30°. Moreover, the LYP steel has a better performance than the A36 steel walls. In doing so, the exact influence of the parameters on the behavior of the models is investigated in the next sections.

To have a fair comparison, the load has been normalized with  $(t.F_y)$ . As shown in Fig. 7, the LYP walls showed a

**Table 3** Comparing the results of walls to investigate the effect of angle  $\theta$  on the wall’s behavior

	Models	$\Delta_s$	$V_s$	$\Delta_y$	$V_u$	K	E	$\mu$	$\Omega$	$R_u$
wall with $\theta=i$ wall with $\theta=30^\circ$	DC-1-45-A	1.13	1.08	1.01	0.95	0.94	0.97	0.99	0.88	0.88
	DC-1-60-A	1.19	1.04	1.09	0.93	0.85	0.95	0.91	0.90	0.87
	DC-1-90-A	1.50	1.14	1.28	0.97	0.76	0.98	0.78	0.85	0.76
wall with $\theta=i$ wall with $\theta=30^\circ$	DC-1-45-L	1.35	1.26	1.04	0.98	0.94	0.98	0.96	0.78	0.76
	DC-1-60-L	1.42	1.27	1.12	0.95	0.85	0.96	0.90	0.75	0.71
	DC-1-90-L	2.08	1.35	1.42	0.91	0.64	0.91	0.70	0.67	0.56

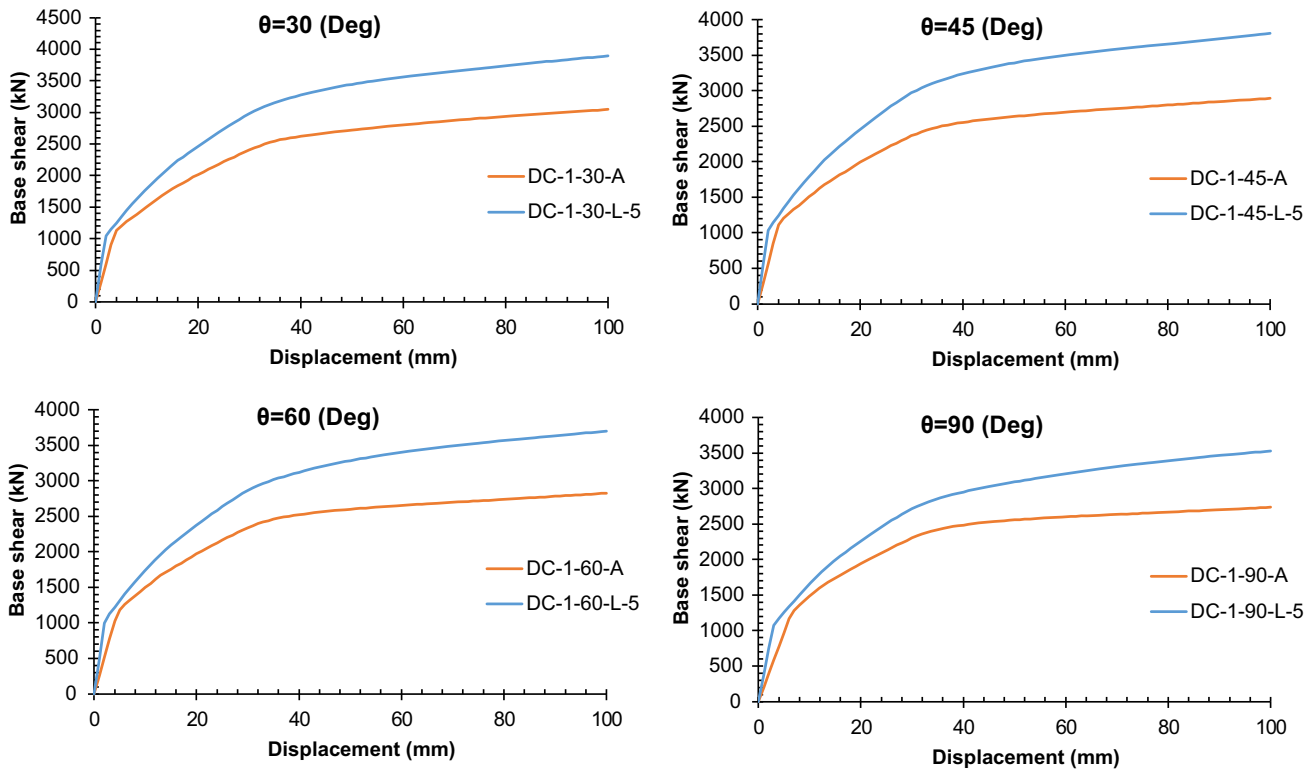


**Fig. 9** Comparing the pushover curve of the FE models considering the LYP effect

**Table 4** Comparing the results of walls to investigate the effect of LYP steel on the wall’s behavior

	Models	$\Delta_s$	$V_s$	$\Delta_y$	$V_u$	$\mu$	$\Omega$	$R_u$
LYP /A36	30	0.38	0.73	0.66	1.28	1.52	1.75	2.14
	45	0.45	0.85	0.67	1.31	1.49	1.54	1.85
	60	0.46	0.89	0.67	1.31	1.49	1.46	1.76
	90	0.45	0.83	0.67	1.28	1.50	1.54	1.84

better performance in the case of ultimate strength and dissipating energy. Also, for both walls with A36 and LYP steels, the walls with a corrugated angle of  $30^\circ$  possess greater performance. The lowest curve is obtained by corrugated walls with an angle of  $90^\circ$ .

### 4.2 Effect of the Corrugated Angle $\theta$ on the Behavior of Walls

Figure 8 illustrates the share of the infill plate considering the corrugated angle,  $\theta$ , in resisting lateral loading. As

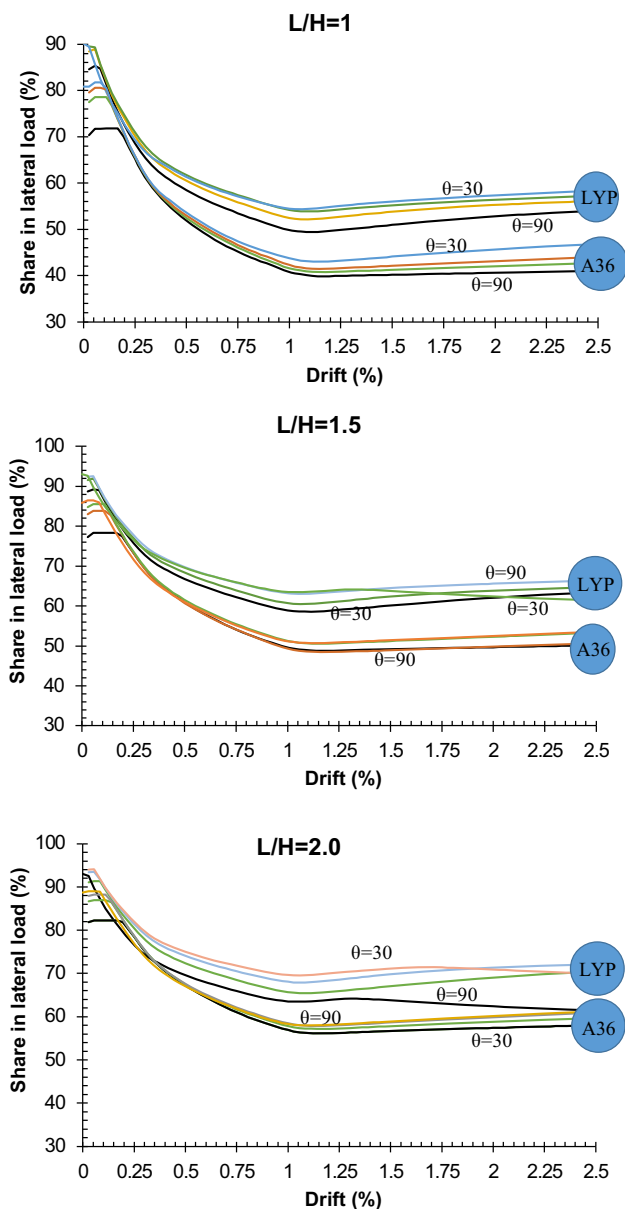


Fig. 10 Comparing the effect of materials in the share of infill plate in load-bearing

shown in Fig. 8, the corrugated angle affects the behavior of walls with A36 and LYP steels. The comparison results driven by the pushover curves of FE results, and Table 2, are listed in Table 3. The results indicate that by increasing the angle  $\theta$ , the seismic performance of the wall decreases. The effect of  $\theta$  on the structural parameters of walls with LYP steel is more than on walls with A36 steel. For both walls, by the  $\theta = 90^\circ$ , the stiffnesses of the walls are significantly reduced. The elastic stiffness of the walls is reduced by 24% for A36-wall by changing the  $\theta$  from  $30^\circ$  to  $\theta = 60^\circ$ , whereas it is reduced by 36% for LYP walls. Also, it has a similar effect on the  $R_u$  and  $\Omega$ . The  $R_u$  for A-36 walls is reduced by 24% by changing the  $\theta = 30^\circ$  to

$\theta = 60^\circ$ , whereas it is reduced by 56% for LYP walls. This decrease is considerable. The  $\theta$  has a lower effect on the ultimate strength,  $V_u$ , and energy absorption,  $E$ , in comparison with other structural parameters. Increasing the  $\theta$  reduces 2 to 9% of the  $V_u$  and  $E$ .

In addition to the  $\theta$ , the L/H ratio also affects the share of the infill plate (which will be examined in the next section) in lateral loading. For all L/H ratios, by increasing the  $\theta$ , the share of the infill plate in lateral load-bearing is reduced. For L/H = 1 with A36 materials, during drift equals 0.23 to 0.27, the  $\theta$  does not affect the share of infill plate in load-bearing that is drift = 0.1 to 0.255 for wall with LYP steels. As the L/H ratio increases, the interval between the effect of angle on the shear share of the infill plate increases; of course, LYP-steel sheets are less affected.

### 4.3 Effect of Infill Plate’s Materials Properties

In Fig. 9, the comparison of the wall to investigate the effect of the infill plate’s materials properties on the behavior of walls is plotted. As shown in Fig. 9, the LYP materials improve the behavior of walls.

According to the structural parameters listed in Table 4, using the LYP steel instead of A36, the ultimate strength is increased by around 31%. But, the  $\Delta_s$  and  $V_s$  are reduced by 55 to 62% and 27 to 17%, respectively. Reducing the parameters leads the structures to yield to reach better performance. Therefore, the  $\mu$ ,  $\Omega$ , and  $R_u$  are improved by around 50, 54 to 75%, and 1.84 to 2.14 times, respectively. This comparison confirms the ability of the LYP to improve the behavior of the wall.

Figure 10 reveals that by changing the materials from A36 to LYP, the share of the infill plate in load-bearing is considerably amplified. As the share of the infill plate in load-bearing is raised, the susceptibility of hinge formation in columns is reduced. Therefore, it is expected that by using LYP steel for the infill plate, the safety of the structure is enhanced.

### 4.4 Investigating the L/H Ratio on the Behavior of the Wall

In Fig. 11, the response of walls has been compared to investigate the L/H aspect ratio. As the L/H ratio increases, the pushover diagram moves upwards, which increases the seismic parameters. Therefore, by increasing the L/H ratio with a constant thickness, which leads to an increase in the slender ratio of the infill plate, not only does it not reduce seismic performance, but it also improves the seismic performance of the wall. In DC-2-30-A and DC-1.5-30-A models, compared to the DC-1-30-A model, the resistance has increased by about 33% and 13%, respectively; also,



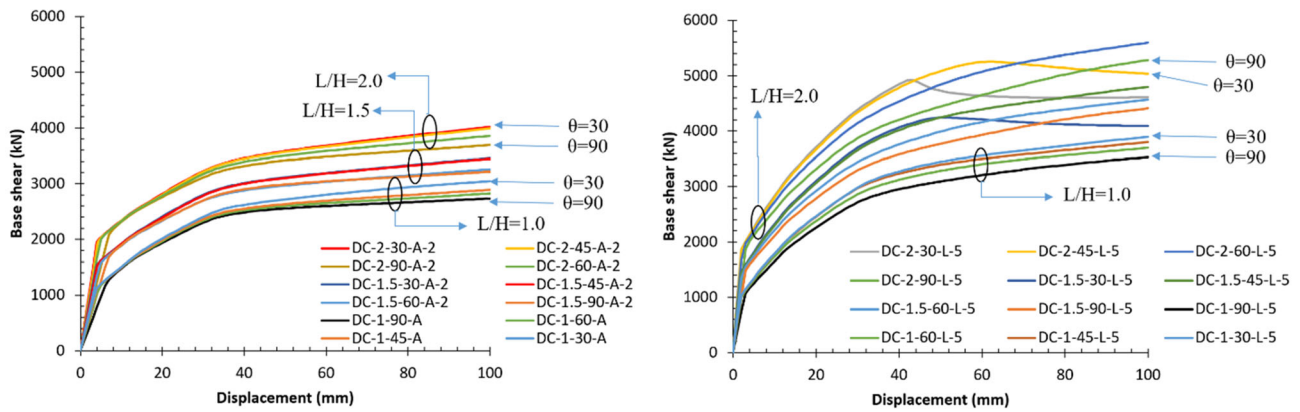


Fig. 11 Comparing the pushover curve of the FE models considering the L/H ratio

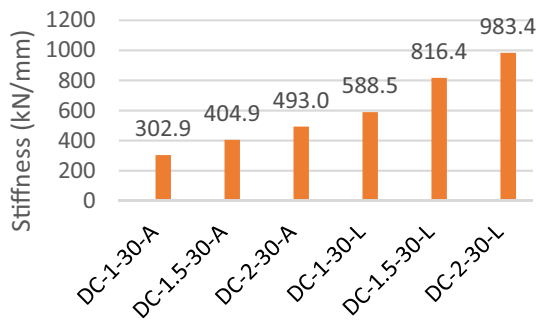


Fig. 12 Stiffness diagram of models with a wave angle of 30 degrees

for all models by doubling the dimensional ratio (L/H), we have seen an increase in resistance of about 25% to 35%. According to Fig. 11, with increasing the aspect ratio, we see an increase in sheet stiffness, which was 66% and 33% in DC-2–30-A and DC1.5–30-A models compared to DC-1-30-A, respectively. As shown in Fig. 12, the stiffness of the LYP steel models (with double and a half thickness) is about twice that of the A36 steel models. According to the results, it can be explained that increasing the length of the filler plate, in any case, is more important than increasing the thickness. However, increasing the thickness of the sheet has a greater effect on the stiffness of the samples. It is suggested to use of wall with a L/H ratio greater than 1 for both A36 and LYP steel walls.

### 5 Proposed Relation to Predicting the Ultimate Strength

Figure 13 shows the load vs. drift diagram for all models. According to Fig. 13, the frame behaves almost the same for all dimensional ratios (L/H). However, with the increase of the dimensional ratio (L/H) for all models, we see an increase in the contribution of the filler plate to the frame, which is more in LYP steel.

Therefore, according to Refs. [41, 42], the ultimate strength of the boundary frame is measured as Eq. (1) and (2). The shear force of the frame after the formation of the plastic joint in the columns,  $F_f$ , was introduced as the shear capacity or ultimate shear force of the frame. The displacement  $\Delta_f$  was corresponded to the displacement of the elastic limit (beginning of the plastic displacement) of the frame and considered:

$$\Delta_f = \frac{M_{fp}H^2}{6E_cI_c} \tag{1}$$

$$F_f = \frac{4M_{fp}}{H} \tag{2}$$

where  $E_c$  is the modulus of elasticity of columns,  $I_c$  is the moment of inertia of the column, and  $M_{fp}$  is the lowest plastic moment capacity.

Based on the fitting of the results, the following relation is proposed for predicting the ultimate strength of the infill plate

$$F_w = L.t_pF_{y,wall} \left( 0.01 + \frac{L}{H\sin\theta} \frac{F_{y,col}}{F_{y,wall}} \right) \tag{3}$$

where  $F_{y,col}$  and  $F_{y,wall}$  are the yielding stress of columns and infill wall, respectively, and  $t_p$  is the total thickness of the double corrugated infill plate.

Therefore, the ultimate strength of the double corrugated SPSW is proposed as follows:

$$F_u = F_f + F_w \tag{4}$$

As shown in Fig. 14, the simple proposed relation (4) predicts the ultimate strength of the double corrugated SPSW with good accuracy. Since the proposed relation predicts the ultimate strength lower than FE modeling, it would be conservative in the design of the system.

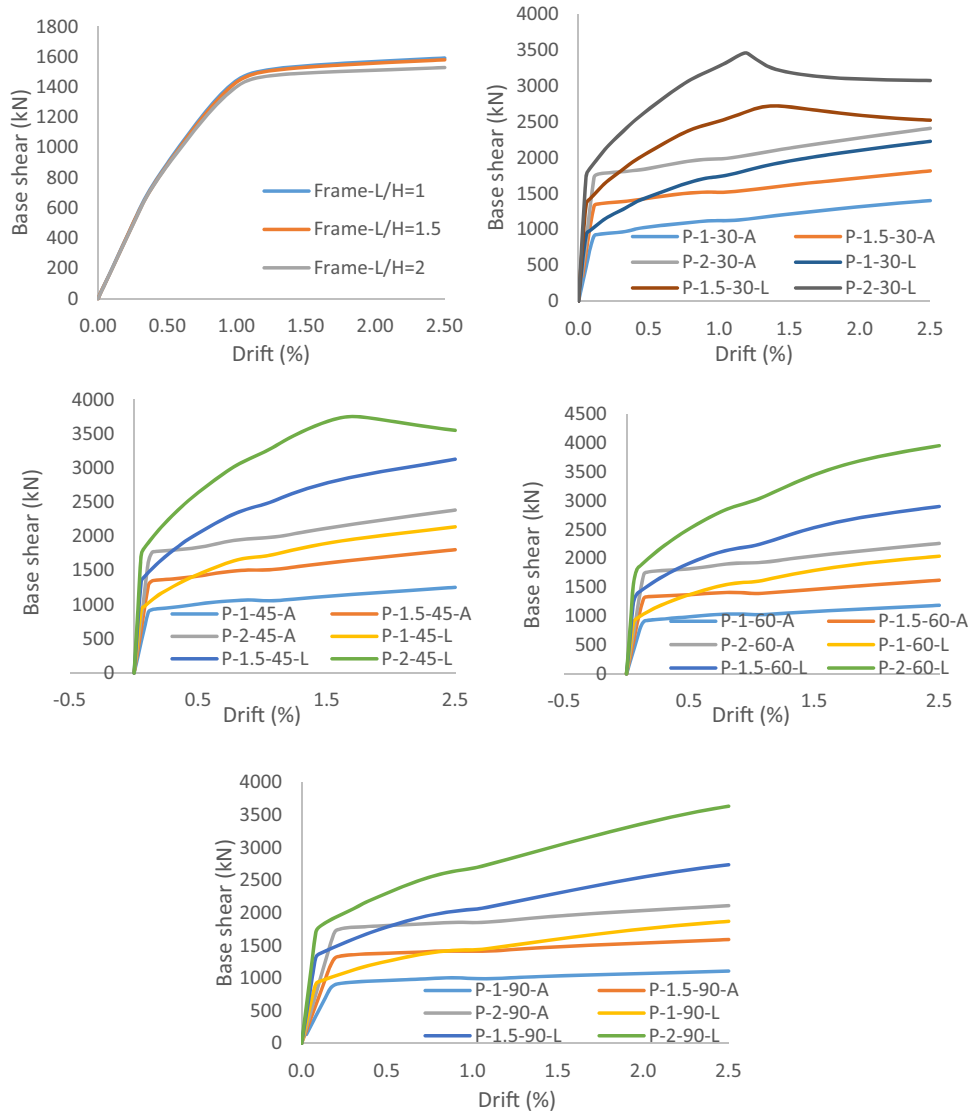


Fig. 13 Interaction of wall-frame

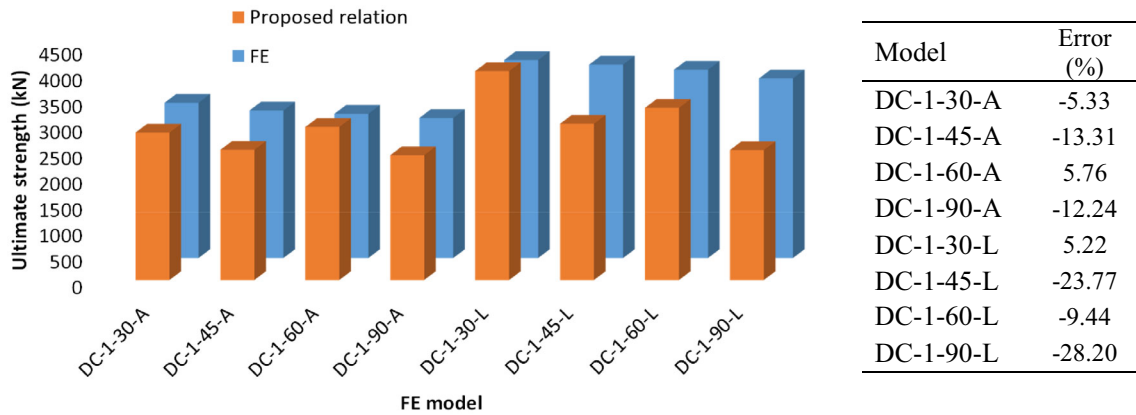


Fig. 14 Comparing the FE results with the proposed relation

## 6 Conclusions

To increase the buckling resistance of the infill steel plate, its thickness can be increased, but with the increase in thickness, the amount of stress transferred to the boundary frame increases. For this reason, made the assumption of equal capacity where increased thickness and decreased yield stress. In this paper, the effects of the steel type (A36 and LYP) of the infill plate on the behavior of the double corrugated steel plate shear walls were investigated. The results are summarized as follows:

- The results showed that LYP steel improves the seismic behavior of corrugated double walls.
- In walls with both materials (A36 and LYP), by increasing the  $\theta$ , the seismic performance of the wall is reduced. But The effect of  $\theta$  on the structural parameters of walls with LYP steel is more than that of walls with A36 steel.
- For a wall with both materials (A36 and LYP), by  $\theta = 90^\circ$ , the strength and stiffness of the wall are significantly reduced.
- The elastic stiffness of walls is reduced by 24% for A36-walls by changing the  $\theta$  from  $30^\circ$  to  $\theta = 60^\circ$ , whereas it is reduced by 36% for LYP walls. Also, it has a similar effect on  $R_u$  and  $\Omega$ . The  $R_u$  for A36 walls is reduced by 24% by changing the  $\theta = 30^\circ$  to  $\theta = 60^\circ$ , whereas it is reduced by 56% for LYP walls.
- The  $\theta$  has a lower effect on the ultimate strength,  $V_u$ , and energy absorption,  $E$ , in comparison with other structural parameters. Increasing the  $\theta$  reduces 2% to 9% of the  $V_u$  and  $E$ .
- For  $L/H = 1$  with A36 materials, during drift equals 0.23 to 0.27, the  $\theta$  does not affect the share of infill plate in load-bearing that is drift = 0.1 to 0.255 for wall with LYP steel.
- As the  $L/H$  ratio increases, the seismic parameters improve.
- Increasing the  $L/H$  ratio, which leads to an increase in the slender ratio of the infill plate, not only does not reduce seismic performance, but also improves the seismic performance of the wall. It is suggested to use of wall with a  $L/H$  ratio greater than 1 for both the A36 wall and the LYP wall.
- A practical relation was proposed for predicting the ultimate strength of the double corrugated SPSW with good accuracy.

**Funding** Open access funding provided by HEAL-Link Greece. This research received no external funding.

**Data availability** The data used to support the findings of this study are included within the article.

## Declarations

**Conflict of interest** The authors declare that they have no conflicts of interest.

**Open Access** This article is licensed under a Creative Commons Attribution 4.0 International License, which permits use, sharing, adaptation, distribution and reproduction in any medium or format, as long as you give appropriate credit to the original author(s) and the source, provide a link to the Creative Commons licence, and indicate if changes were made. The images or other third party material in this article are included in the article's Creative Commons licence, unless indicated otherwise in a credit line to the material. If material is not included in the article's Creative Commons licence and your intended use is not permitted by statutory regulation or exceeds the permitted use, you will need to obtain permission directly from the copyright holder. To view a copy of this licence, visit <http://creativecommons.org/licenses/by/4.0/>.

## References

1. Salimi SM, Rahimi S, Hoseinzadeh M, Kontoni D-PN, Ebadi-Jamkhaneh M (2021) Numerical 3D finite element assessment of bending moment-resisting frame equipped with semi-disconnected steel plate shear wall and yielding plate connection. *Metals* 11(4):604. <https://doi.org/10.3390/met11040604>
2. Mashhadiali N, Gholhaki M, Kheyroddin A, Zahiri-Hashemi R (2016) Vulnerability investigation in 3D shear wall, X-braced and moment frame subjected to progressive collapse. *Int J Civil Eng.* 14(8): 595–608. <http://ijce.iust.ac.ir/article-1-1383-en>
3. Berman JW (2011) Seismic behavior of code designed steel plate shear walls. *Eng Struct* 33(1):230–244. <https://doi.org/10.1016/j.engstruct.2010.10.015>
4. Doan QH, Lee D, Lee J, Kang J (2019) Design of buckling constrained multiphase material structures using continuum topology optimization. *Meccanica* 54:1179–1201. <https://doi.org/10.1007/s11012-019-01009-z>
5. Nguyen M-N, Hoang V-N, Lee D (2023) Multiscale topology optimization with stress, buckling and dynamic constraints using adaptive geometric components. *Thin Walled Struct* 183:110405. <https://doi.org/10.1016/j.tws.2022.110405>
6. Shafaei S, Ayazi A, Farahbod F (2016) The effect of concrete panel thickness upon composite steel plate shear walls. *J Constr Steel Res* 117:81–90. <https://doi.org/10.1016/j.jcsr.2015.10.006>
7. Ebadi-Jamkhaneh M, Kontoni D-PN (2022) Numerical finite element investigation of thin steel shear walls retrofitted with CFRP layers under reversed cyclic loading. *J Build Pathol Rehabil* 62(7):1–10. <https://doi.org/10.1007/s41024-022-00200-2>
8. Jahanpour A, Moharrami H, Aghakoochak A (2011) Evaluation of ultimate capacity of semi-supported steel shear walls. *J Constr Steel Res* 67(6):1022–1030. <https://doi.org/10.1016/j.jcsr.2011.01.007>
9. Hosseinzadeh L, Mofid M, Emami F (2017) Experimental investigation on the behavior of corrugated steel shear wall subjected to the different angle of trapezoidal plate. *Struct Design Tall Spec Build* 26(17):e1390. <https://doi.org/10.1002/tal.1390>
10. Emami F, Mofid M, Vafai A (2013) Experimental study on cyclic behavior of trapezoidally corrugated steel shear walls. *Eng Struct* 48:750–762. <https://doi.org/10.1016/j.engstruct.2012.11.028>

11. Kalali H, Ghazijahani T, Hajsadeghi M, Zirakian T, Alaei F (2016) Numerical study on steel shear walls with sinusoidal corrugated plates. *Lat Am J Solids Struct* 13(15):2502–2514. <https://doi.org/10.1590/1679-78252837>
12. Yadollahi Y, Pakar I, Bayat M (2015) Evaluation and comparison of behavior of corrugated steel plate shear walls. *Lat Am J Solids Struct* 12(4):763–786. <https://doi.org/10.1590/1679-78251469>
13. Kalali H, Hajsadeghi M, Zirakian T, Alaei F (2015) Hysteretic performance of SPSWs with trapezoidally horizontal corrugated web-plates. *Steel Compos Struct* 19(2):277–292. <https://doi.org/10.12989/scs.2015.19.2.277>
14. Hosseinpour E, Baharom S, Yadollahi Y (2015) Evaluation of steel shear walls behavior with sinusoidal and trapezoidal corrugated plates. *Adv Civil Eng*. <https://doi.org/10.1155/2015/715163>
15. Bergman S, Reissner H (1929) Neuere probleme aus der flugzeugstatik. *Zeitschrift Flugtech und Mororluftsch* 20:475–481
16. Easley JT, McFarland DE (1969) Buckling of light-gage corrugated metal shear diaphragms. *J Struct Div* 95(7):1497–1516. <https://doi.org/10.1061/JSDEAG.0002313>
17. Easley JT (1975) Buckling formulas for corrugated metal shear diaphragms. *J Struct Div* 101(7):1403–1417. <https://doi.org/10.1061/JSDEAG.0004095>
18. Guo T, Sause R (2014) Analysis of local elastic shear buckling of trapezoidal corrugated steel webs. *J Constr Steel Res* 102:59–71. <https://doi.org/10.1016/j.jcsr.2014.06.006>
19. Tong J, Guo Y (2015) Elastic buckling behavior of steel trapezoidal corrugated shear walls with vertical stiffeners. *Thin Walled Struct* 95:31–39. <https://doi.org/10.1016/j.tws.2015.06.005>
20. Dou C, Jiang Z, Pi Y, Guo Y (2016) Elastic shear buckling of sinusoidally corrugated steel plate shear wall. *Eng Struct* 121:136–146. <https://doi.org/10.1016/j.engstruct.2016.04.047>
21. Hosseinzadeh L, Mofid M, Aziminejad A, Emami F (2017) Elastic interactive buckling strength of corrugated steel shear wall under pure shear force. *Struct Design Tall Special Build* 26(8):e1357. <https://doi.org/10.1002/tal.1357>
22. Tang G, Yin L, Guo X, Cui J (2015) Finite element analysis and experimental research on mechanical performance of bolt connections of corrugated steel plates. *Int J Steel Struct* 15(1):193–204. <https://doi.org/10.1007/S13296-015-3014-4>
23. Tong J, Guo Y (2018) Shear resistance of stiffened steel corrugated shear walls. *Thin Walled Struct* 127:76–89. <https://doi.org/10.1016/j.tws.2018.01.036>
24. Dou C, Pi Y, Gao W (2018) Shear resistance and post-buckling behavior of corrugated panels in steel plate shear walls. *Thin Walled Struct* 131:816–826. <https://doi.org/10.1016/j.tws.2018.07.039>
25. Farzampour A, Mansouri I, Hu JW (2018) Seismic behavior investigation of the corrugated steel shear walls considering variations of corrugation geometrical characteristics. *Int J Steel Struct* 18:1297–1305. <https://doi.org/10.1007/s13296-018-0121-z>
26. Qiu J, Zhao QH, Yu C, Li ZX (2018) Experimental studies on cyclic behavior of corrugated steel plate shear walls. *J Struct Eng*. [https://doi.org/10.1061/\(ASCE\)ST.1943-541X.0002165](https://doi.org/10.1061/(ASCE)ST.1943-541X.0002165)
27. Cao Q, Huang JY (2018) Experimental study and numerical simulation of corrugated steel plate shear walls subjected to cyclic loads. *Thin Walled Struct* 127:306–317. <https://doi.org/10.1016/j.tws.2018.01.042>
28. Shon S, Yoo M, Lee S (2017) An experimental study on the shear hysteresis and energy dissipation of the steel frame with a trapezoidal-corrugated steel plate. *Materials* 10(3):261. <https://doi.org/10.3390/ma10030261>
29. Zhang W, Mahdavian M, Li Y, Yu C (2017) Experiments and simulations of cold-formed steel wall assemblies using corrugated steel sheathing subjected to shear and gravity loads. *J Struct Eng*. [https://doi.org/10.1061/\(ASCE\)ST.1943-541X.0001681](https://doi.org/10.1061/(ASCE)ST.1943-541X.0001681)
30. Emami F, Mofid M (2014) On the hysteretic behavior of trapezoidally corrugated steel shear walls. *Struct Design Tall Spec Build* 23(2):94–104. <https://doi.org/10.1002/tal.1025>
31. Kontoni D-P N, Ghamari A, Mahmudi S (2022) Investigation of the fire effect on the behavior of corrugated steel plate shear walls considering environmental aspects. 3rd International Conference on Environmental Design (ICED2022). 22–23 October, Hybrid (Athens, Greece and Virtual), IOP Conference Series: Earth and Environmental Science 1123 012063:1–10. <https://doi.org/10.1088/1755-1315/1123/1/012063>
32. Tong J, Guo Y, Zuo J (2018) Elastic buckling and load-resistant behaviors of double corrugated-plate shear walls under pure in-plane shear loads. *Thin Walled Struct* 130:593–612. <https://doi.org/10.1016/j.tws.2018.06.021>
33. Tong J, Guo Y, Zuo J, Goa J (2020) Experimental and numerical study on shear resistant behavior of double-corrugated-plate shear walls. *Thin Walled Struct* 147:106485. <https://doi.org/10.1016/j.tws.2019.106485>
34. Tong J, Guo Y, Zuo J, Goa J (2020) Ultimate shear resistance and post-ultimate behavior of double-corrugated-plate shear walls. *J Constr Steel Res* 165:105895. <https://doi.org/10.1016/j.jcsr.2019.105895>
35. AISC-Design Guide 20, Sabelli R, Bruneau M (2006) Steel Plate Shear Walls. American Institute of steel construction. INC. <https://www.aisc.org/Design-Guide-20-Steel-Plate-Shear-Walls>
36. Bahrebar M, Lim JBP, Clifton GC, Zirakian T, Shahmohammadi A, Hajsadeghi M (2020) Response assessment and prediction of low yield point steel plate shear walls with curved corrugated web plates and reduced beam sections. *Structures* 28:1729–1745. <https://doi.org/10.1016/j.istruc.2020.09.071>
37. ABAQUS (2011). ABAQUS user's manual, version 6.11. Dassault Systemes Simulia Corporation, Providence, RI, USA
38. Keykhosro Kiani B, Hosseini Hashemi B, Torabian S (2020) Optimization of slit dampers to improve energy dissipation capacity and low-cycle-fatigue performance. *Eng Struct* 214:110609. <https://doi.org/10.1016/j.engstruct.2020.110609>
39. Keykhosro Kiani B, Hosseini Hashemi B (2021) Development of a double-stage yielding damper with vertical shear links. *Eng Struct* 246:112959. <https://doi.org/10.1016/j.engstruct.2021.112959>
40. ASCE 7, ASCE, SEI 7–22 (2022) Minimum design loads for buildings and other structures. Am Soc Civil Eng Virginia. <https://doi.org/10.1061/9780784415788>
41. Khaloo A, Ghamari A, Foroutani M (2021) On the design of stiffened steel plate shear wall with diagonal stiffeners considering the crack effect. *Structures* 31:828–841. <https://doi.org/10.1016/j.istruc.2021.02.027>
42. Khaloo A, Foroutani M, Ghamari A (2019) Influence of diagonal stiffeners on the response of steel plate shear walls (SPSWs) considering crack propagation. *Bull Earthquake Eng* 17:5291–5312. <https://doi.org/10.1007/s10518-019-00685-2>